IOP Publishing Journal of Physics D: Applied Physics
J. Phys. D: Appl. Phys. **54** (2021) 025105 (7pp) https://doi.org/10.1088/1361-6463/abb553

Optical characterization of nanostructured $\beta - FeSi_2$ layers obtained by Fe^+ implantation

Cecilia Salinas-Fuentes[1,2], **Angélica Hernández-Zanabria**[3], **Yuriy Kudriavtsev**[1,4] and **Juan-Carlos Cheang-Wong**[2]

[1] Nanoscience and Nanotechnology Doctorate Program, Center for Research and Advanced Studies of the National Polytechnic Institute, CINVESTAV-IPN, Av. IPN n. 2508, Col. San Pedro Zacatenco, Mexico City, C.P. 07360, Mexico
[2] Instituto de Física, Universidad Nacional Autónoma de México, Cd. Universitaria, Coyoacan, Ciudad de México, 04510, México
[3] Autonomous Hidalgo State University, Tepeji del Río de Ocampo, Hidalgo, 42855, México
[4] Solid State Electronics section, Electrical Engineering Department, Center for Research and Advanced Studies of the National Polytechnic Institute, CINVESTAV-IPN, Av. IPN n. 2508, Col. San Pedro Zacatenco, Mexico City, C.P. 07360, Mexico

E-mail: car_cecilia.salinas@cinvestav.mx

Received 12 June 2020, revised 17 August 2020
Accepted for publication 4 September 2020
Published 19 October 2020

Abstract

In this work, we present a comprehensive analysis of nanostructured $\beta - FeSi_2$ layers obtained by 40 keV Fe ion implantation in silicon, followed by rapid thermal annealing. A series of chemical, structural and optical characterizations of the samples were performed. Our results establish the formation of a 26.6 nm thick layer consisting of $\beta - FeSi_2$ nanocrystals, with an average size of 4.8 nm, embedded in the Si substrate. Optical excitation of the sample leads to a photoluminescence signal with an extremely narrow peak (1 nm full width at half maximum) at 1456 nm. This sharp emission is comparable with the radiation of semiconductor lasers and therefore, this $\beta - FeSi_2$ nanostructured layer is of interest for the fabrication of new optoelectronic devices in the near-infrared region.

Keywords: nanostructure, photoluminescence, beta-iron disilicide, ion implantation

(Some figures may appear in colour only in the online journal)

1. Introduction

$\beta - FeSi_2$ compounds have been investigated thoroughly in the literature, due to their promising semiconducting properties, making them serious candidates for the fabrication of new near-infrared optoelectronic devices on silicon, like photonic crystals. Indeed, $\beta - FeSi_2$ is a direct band gap semiconductor, with a gap between 0.83 and 0.92 eV, which corresponds to a wavelength between 1494 and 1348 nm, very near the absorption minimum wavelength for silica optical fibers ($\simeq$1550 nm) [1]. Moreover, $\beta - FeSi_2$ has a large optical absorption coefficient (over 10^5 cm^{-1}) [2–4]. Finally, the constitutive elements Fe and Si are easily found in nature and they can be safely manipulated.

Due to all these remarkable properties, $\beta - FeSi_2$ is being studied actively in the literature, especially in regard to possible optical applications. In particular, in the most recent literature, Ishiyama *et al* [5] discuss possible applications as photonic devices compatible with existing complementary metal-oxide-semiconductor (CMOS) technology, because $\beta - FeSi_2$ has infrared emission. Terai *et al* [6] and Wang *et al* [7] argue that since $\beta - FeSi_2$ shows a photoluminescence

around 1.54 μm it can be used for optoelectronic and photovoltaic applications. Rajesh *et al* [8] expound on the fact that for the direct band gap and for the large optical absorption coefficient, $\beta - FeSi_2$ has great potential for applications like telecommunication devices based on silicon, photo sensors, solar cells and thermoelectric generators (see also [9]).

Previously, different techniques for the fabrication of $\beta - FeSi_2$ have been used, such as ion beam synthesis (IBS), molecular beam epitaxy (MBE) and metal-organic chemical vapor deposition (MOCVD) [10]. With these methods one can obtain different structures, ranging from thin films [11] to nanoparticles [12] and heterojunction thin films [13]. It has also been observed that the photoluminescence signal may vary depending on the method used. Therefore it is of primary importance to obtain a type of structure with a stable optical response, allowing its use in the fabrication of new optoelectronic devices. In this regard, Rysbaev *et al* [14] have recently started an investigation on nanosized films of silicides obtained by ion beam implantation. The advantages of the ion beam implantation technique over other methods are the repeatability of the samples, since the distribution of the implanted ions can be controlled with high accuracy, alongside the fact that, with the use of a mask, the ion implantation can be performed in specific areas of a wafer, thus encouraging its application in thin silicon technology, which is very useful for device fabrication. This makes this technique the method of choice for the manufacture of silicon integrated circuits for example.

Previous works developed by other authors have focused on the characterization of the structural properties of $\beta - FeSi_2$ by means of Rutherford backscattering (RBS), Raman spectroscopy, and x-ray diffraction (XRD) [15, 16]. However, in order to have a complete understanding of the properties of $\beta - FeSi_2$, we need to combine the existing results with further analysis, involving other techniques.

For all these reasons, in this work a comprehensive characterization of $\beta - FeSi_2$ nanocrystals obtained by ion beam implantation is presented, focusing on the photoluminescence (PL) properties that are relevant for the fabrication of optoelectronic devices in the near-infrared region.

2. Experimental setting

$\beta - FeSi_2$ nanocrystals have been obtained by ion beam implantation at high fluence (1×10^{17} ions cm^{-2}) and low energy (40 keV). The motivation for using high-fluence implantation is because this provokes concentrations that exceed the solubility limit of the Fe ions implanted in the silicon matrix. Annealing this oversaturated system leads to the formation of $\beta - FeSi_2$ nanoparticles.

Commercially available crystalline Si (111) wafers were implanted with 40 keV Fe ions at a fluence of 1×10^{17} ions cm^{-2}. The Si wafers were cut into small square pieces (1×1 cm^2) and subsequently they were ultrasonically cleaned in ethanol for 5 minutes. Rapid thermal annealing (RTA) was performed at 900 °C for 8 min under a chromatographic nitrogen (N_2) atmosphere. After RTA the samples

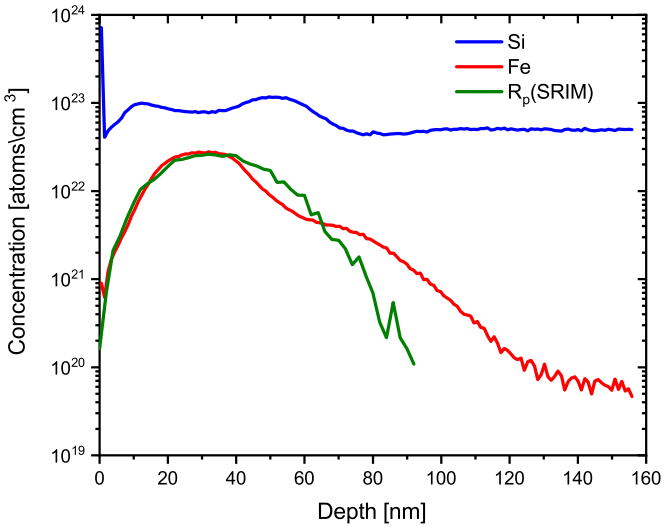

Figure 1. SIMS concentration depth profiles for the sample prepared by 40 keV Fe ion implantation in Si (1×10^{17} ions cm^{-2}) and annealed in N_2 at 900 °C for 8 min. The red curve corresponds to the Fe profile and the blue curve to the Si one. For comparison the Fe depth profile simulated by SRIM is included (green curve).

were etched with 3 keV Ar ions at normal incidence without sample rotation and approximately 10 nm were removed.

The chemical analysis of the samples was investigated by secondary ion mass spectroscopy (SIMS) by acquisition of a depth profile performed by a TOF-SIMS-5 spectrometer from Ion-TOF GmbH. A 2 keV cesium ion beam for sputtering and a 30 keV Bi^+ pulsed ion beam were used for analysis of the central part of the sputter crater. The angle of incidence was 45° for both ion beams. The sputter crater size was chosen to be 300×300 μm^2 and the area of analysis was a 150×150 μm^2 raster in the center of the sputter crater.

The structural characterization, chemical analysis and PL signal were performed by Raman spectroscopy with an NTEGRA Spectra instrument from NT-MDT with a 100x objective. For structural characterization and chemical analysis a laser excitation at 532 nm was used, while for PL signal the laser excitation was at 473 nm. The exposure time was 60 seconds and the CCD was cooled to −65 °C to obtain the spectrum in the mode of single acquisition.

Morphology of the samples was investigated by atomic force microscopy (AFM) and scanning electron microscopy (SEM). The tapping mode AFM studies were carried out in air by using a Solver Next instrument from NT-MDT. We employed silicon cantilevers with a tip curvature radius of about 10 nm. The micrographs were acquired with a resolution of 512×512 pixels and a scanning frequency of 1 Hz. SEM measurements were performed using a JEOL JSM-7800 F, with secondary electrons with a voltage of 5 kV. The chemical map was obtained by energy dispersive spectroscopy (EDS) at 10 kV. The nanocrystals embedded in a silicon matrix were observed by transmission electron miscroscopy (TEM) (JEM2010 FEG).

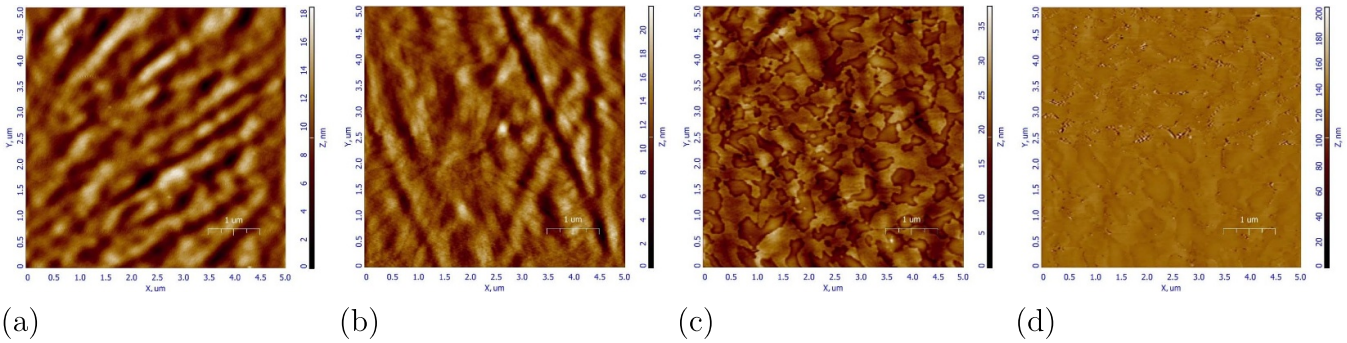

Figure 2. AFM micrographs corresponding to the different stages of the 40 keV Fe ion implanted sample (1×10^{17} ions cm^{-2}): (a) as-implanted sample; (b) after the RTA in N_2 at 900 °C for 8 min; (c) after removing a 10 nm thick layer by Ar^+ etching; (d) after removing a 60 nm thick layer.

3. Results

3.1. SIMS depth profiling

SIMS was used to determine the concentration depth profile of the 40 keV Fe ions implanted in Si substrates and annealed in N_2 at 900 °C for 8 minutes. As shown in figure 1, the Fe peak concentration is located at 32 nm. For comparison purposes, the Fe depth profile simulated by the SRIM code is included [17]. The software describes the transport properties of ions in matter, but no thermal diffusion effects are considered. In this case the simulated Fe concentration profile can be described as a Gaussian-like curve, with a maximum value at around 38 nm, similar to the shape of the experimental curve, as can be observed in figure 1. The in-depth diffusion of the Fe atoms from the surface towards the interior of the Si matrix is induced by the annealing. This explains the observed difference between the green and the red curves in figure 1 after 40 nm.

The observed surface sputtering effect due to the high-fluence ion bombardment is consistent with the simulated results reported by other groups [16]. Indeed, for our 1×10^{17} ions cm^{-2} implanted sample, a similar Fe depth profile as [16] was obtained, with the same maximum value. The Fe profile shows the formation of a new phase between 15 nm and 45 nm in depth scale. This gives us an indication that the thickness of the $\beta - FeSi_2$ layer is around 30 nm. To corroborate this intuition, a Gaussian approximation of the Fe profile was used and the calculated full width at half maximum (FWHM) was 26.6 nm $\pm$ 0.7 nm.

3.2. AFM and SEM analysis

The surface of the implanted samples was characterized by using AFM and SEM-EDS, both before and after the RTA. Moreover, in order to get access to the nanostructured film, a thin layer of about 10 nm was removed after annealing by etching with normal incident 3 keV Ar ions. Figures 2(a) and (b) show, respectively, the AFM images of the samples before and after the rapid thermal annealing. Structuring can be clearly observed on the silicon surface, attenuated by the RTA. The estimated root mean square roughness (R_{rms}) was 3.5 nm and 2.7 nm respectively. Figures 2(c) and (d) show the same sample after etching into two different depths. After removing a 10 nm thick layer the surface structure exhibits a variety of shapes with irregular sizes of the order of μm (figure 2(c)). This morphology is still present even after removing a 60 nm thick layer (figure 2(d)). In this case the estimated root mean square roughness (R_{rms}) was 5.8 nm and 4.6 nm respectively.

The SEM results confirm the presence of the same patterns as described from AFM analysis (see figure 3). The structure observed in AFM and SEM can be attributed to selective sputtering. In fact, the SRIM simulation reveals that the erosion coefficients for silicon and silicide exhibit a clear difference: Y(Si) = 1 atom ion^{-1} and Y($FeSi_2$) = 2.2 atom ion^{-1} respectively. Thus, this structure is produced while removing the sample surface with the Ar^+ plasma etching at differentiated erosion coefficients.

The island morphology observed in figure 3, together with its composition is explained by figure 4, which shows the results of the SEM-EDS analysis associated with the Fe atomic distribution in the silicon substrate. In particular, figure 4(a) is a magnification of a region of the SEM micrograph presented in figure 3(b). The corresponding Si and Fe distributions are shown in figures 4(b) and (c), respectively. Accordingly, the concentration of Fe atoms is clearly higher in those regions corresponding to light grey areas in the SEM micrographs. From the SIMS profile we know that the Fe concentration diminishes at greater depth, and it is for this reason that at 60 nm we observe smaller islands than those at 10 nm. Therefore we can infer that the observed structures are not due to the presence of porosities in the Si matrix, but they are related to the formation of a new compound from the combination of Fe and Si. So far, we argue that the new compound that has been formed is iron disilicide. In the next section, this analysis is complemented with Raman spectroscopy, that proves that iron disilicide is found in its $\beta - FeSi_2$ phase.

3.3. Raman spectroscopy

The study of Raman spectroscopy before and after the annealing at 900 °C yields information about the amorphization and recrystallization of the silicon substrate. Figure 5 shows the Raman spectra obtained before (blue curve) and after

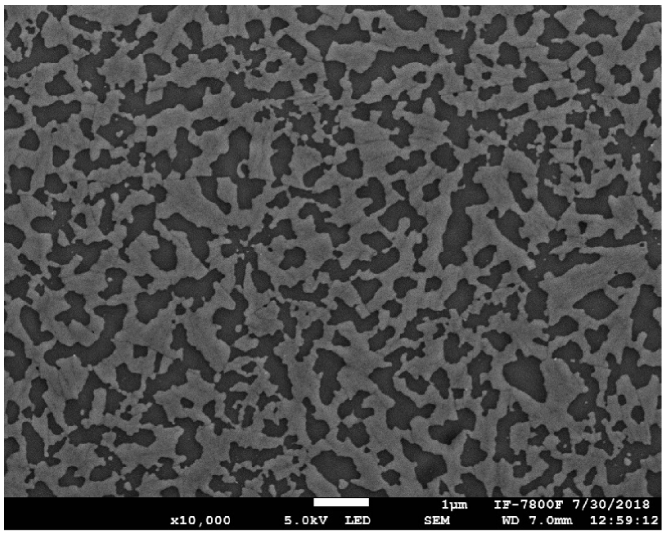

(a)

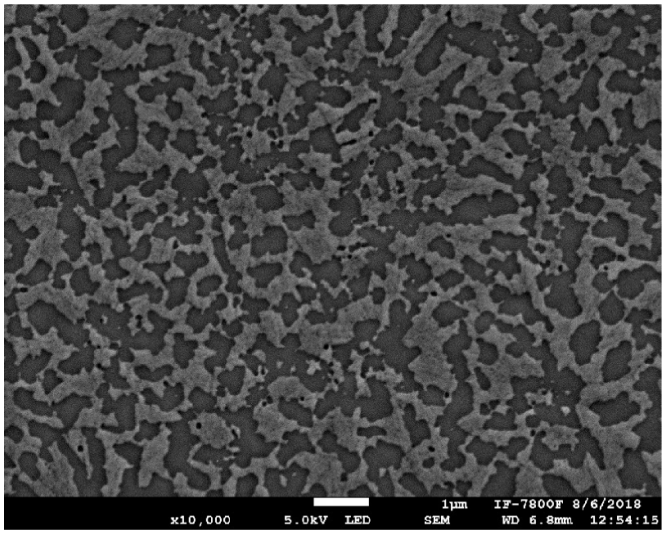

(b)

Figure 3. SEM micrographs of the Ar^+ plasma etched samples after removing a layer of: (a) 10 nm, and (b) 60 nm.

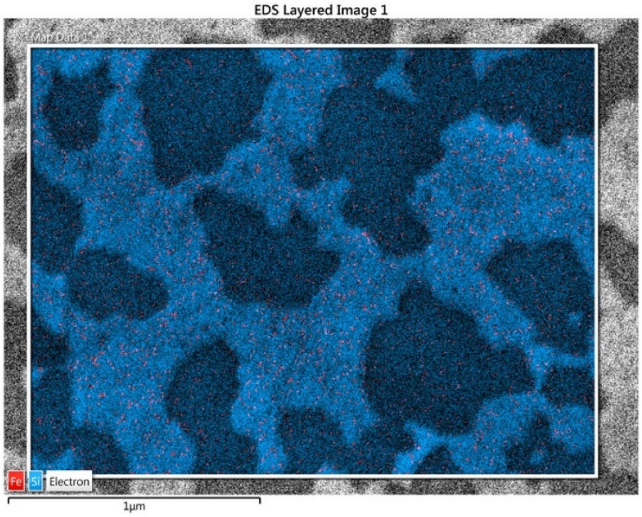

(a)

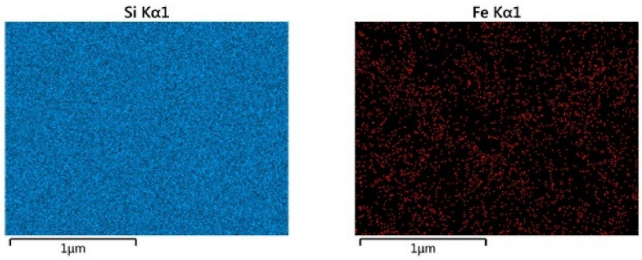

(b) (c)

Figure 4. SEM-EDS analysis associated with the Fe atomic distribution in the Si substrate for the Ar^+ plasma etched sample after removing a layer of 60 nm. (a) The entire analyzed region; (b) Si distribution; (c) Fe distribution.

(red curve) the RTA of the Fe implanted sample. One can observe that before annealing, the shape of the Raman spectrum exhibits two regions. First, a quite broad band, approximately centered at 465 cm^{-1}, which corresponds to the superficial amorphous Si originated by the ion implantation, as discussed in the previous section. The small peak at 521 cm^{-1} is associated with the remaining crystalline Si structure in the as-implanted sample, i.e. the Si amorphization was not complete.

After RTA, the Raman signal clearly shows the 521 cm^{-1} characteristic peak associated with crystalline Si, indicating that annealing at 900 °C induces the recrystallization of the silicon lattice. Additionally, one can observe two small peaks located at 192 cm^{-1} and 247 cm^{-1}; the characteristic peaks of $\beta - FeSi_2$, which are associated with the A_g phonon mode [18–20].

The difference in peak intensity at 521 cm^{-1} can be explained by considering that the crystalline structure (after annealing) has a larger scattering cross section compared to the amorphous sample due to the crystal disorder. The peaks that appear after annealing at 192 cm^{-1} and 247 cm^{-1} are due to the fact that the Fe ions have clustered to form the $\beta - FeSi_2$ and their intensity indicates the relative concentration of silicide in the silicon matrix. This behavior denotes the formation of $\beta - FeSi_2$.

3.4. Photoluminescence

The PL spectrum of the Fe^+-implanted Si sample after the RTA is shown in figure 6. The main feature observed in the room temperature PL spectrum corresponds to an intense peak at 1456 nm (0.852 eV). This PL signal must be attributed to the formation of a $\beta - FeSi_2$ nanostructured layer, because crystalline silicon is an indirect band gap material and no PL emission is expected. This result is quite similar to those reported in previous works, where PL signals in a 0.80 eV

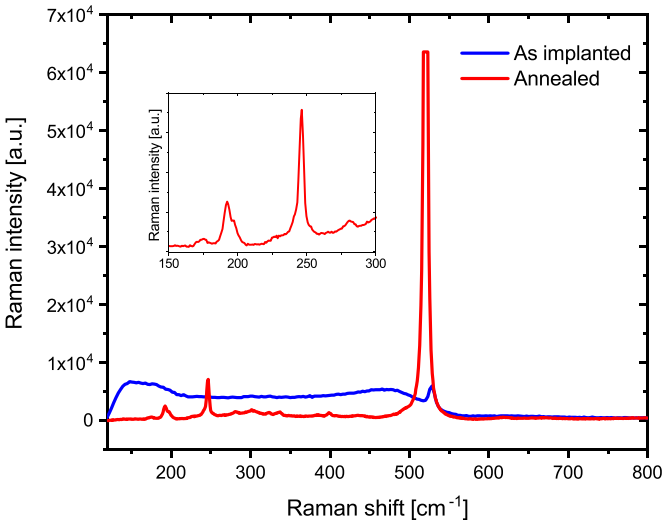

Figure 5. Raman spectra obtained before (blue curve) and after (red curve) the RTA of the Fe implanted sample. The inset shows the two Raman peaks corresponding to the $\beta - FeSi_2$.

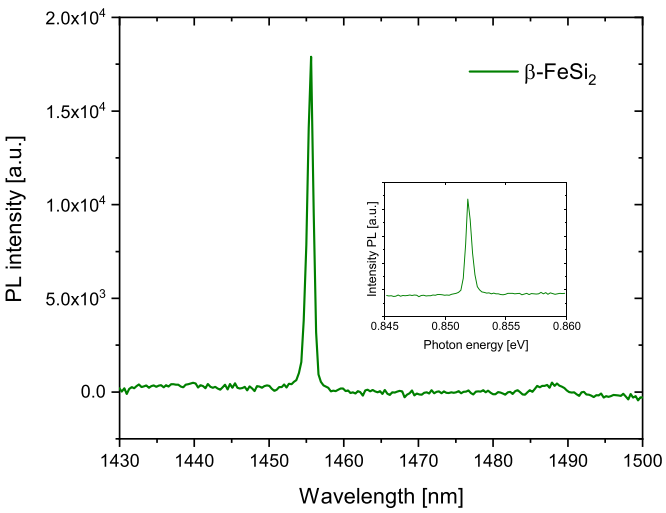

Figure 6. PL spectrum after the RTA at 900 °C. The very thin and intense peak at 1456 nm is associated with the presence of monodisperse $\beta - FeSi_2$ nanocrystals. The inset is a magnification of the peak region, but in a photon energy scale.

$-$ 0.93 eV energy range have been determined. Thus, some authors ascribe the observed fluctuations in the PL peak position to the variation in the $\beta - FeSi_2$ nanocrystal size, ranging from 0.80 eV for large nanocrystals to 0.89 eV for small ones [21, 22]. In the case of nanowires at room temperature (RT), the PL signal centered at 0.96 eV has been reported [23]. Other groups describe a shift in the PL spectrum due to different acquisition temperatures, from 0.93 eV at 3.5 K to 0.87 eV at 300 K [24, 25]. Finally, the PL signal can also depend on the $\beta - FeSi_2$ fabrication method, with PL peaks in the 0.80$-$0.82 eV range [26].

One striking result from the PL spectra shown in figure 6, is that the signal obtained from the nanostructured layer presents an extremely narrow peak, with a FWHM $<$ 1 meV (the

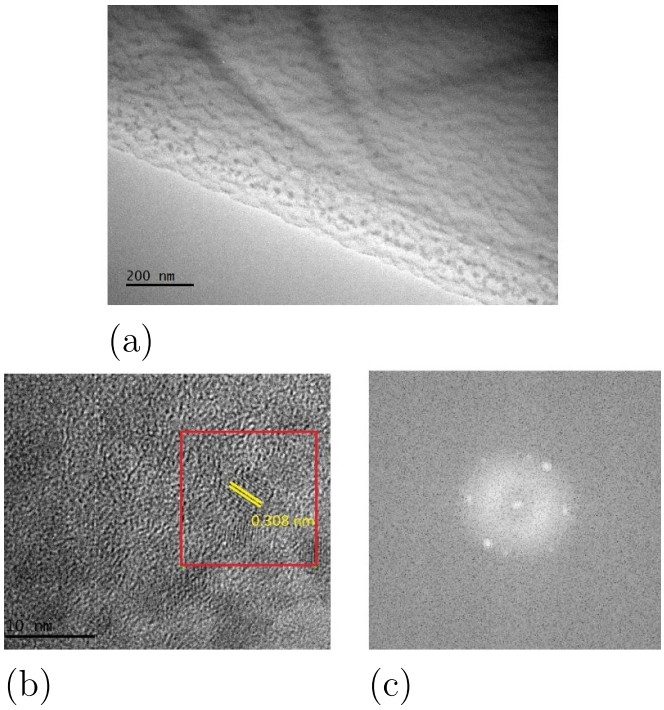

Figure 7. Representative TEM micrographs corresponding to the Fe-implanted Si sample after the RTA. (a) Extended TEM image at high magnification; (b) HRTEM image of a $\beta - FeSi_2$ single-crystal with a size diameter of 5 nm embedded in the amorphous layer; (c) diffraction pattern obtained from the red square area indicated in figure 7(b). The $\beta - FeSi_2$ nanocrystal lattice was indexed to the [220] plane diffraction pattern.

precise value obtained being 1 nm $\pm$ 0.02 nm), a value considerably thinner than the peak widths previously reported for $\beta - FeSi_2$. Low temperature PL measurements (at 10 K) exhibit wide PL signals, with FWHM in the 27$-$52 meV range for different nanostructured layers [27]. Our PL signal is even narrower than that reported for $\beta - FeSi_2$ nanocrystals (FWHM $=$ 19 meV) [28]. By analysis of the PL spectrum and comparison with previous literature, it can be inferred that in our case, the sharp PL peak is due to fairly high monodispersity of the $\beta - FeSi_2$ nanocrystals, as discussed in the next section.

3.5. TEM analysis

In order to obtain a better morphological and structural characterization of the $\beta - FeSi_2$ nanocrystals, a detailed TEM analysis was performed. Figure 7(a) shows an extended view of the $\beta - FeSi_2$ nanocrystals embedded in the silicon matrix, randomly located in the near-surface amorphized Si layer. The depth distribution of the nanocrystals is somewhat narrow, with most nanoparticles laying 40$-$60 nm from the surface. Figure 7(b) shows a representative high resolution transmission electron microscopy (HRTEM) image of a $\beta - FeSi_2$ single-crystal with a size diameter of 4.8 nm $\pm$ 0.49 nm. Additionally, figure 7(c) shows the diffraction pattern obtained from the red square area indicated in figure 7(b). The $\beta - FeSi_2$ nanocrystal lattice was indexed to the [220] plane, with an interplane istance of 3.08 Å (JCPDS database,

No. 01-071-0642). Our results show the formation of spherical nanocrystals with a monodisperse size distribution, with a diameter of approximately 5 nm, which is consistent with the PL signal obtained. Our method allows the fabrication of homogeneously shaped nanocrystals exhibiting an intense PL signal and therefore it can be competitive with other methods aiming for PL signal enhancements [29–33].

4. Conclusions

In this work, the formation of $\beta - FeSi_2$ nanostructured layers by low-energy and high-fluence Fe^+ implantation into Si substrates has been demonstrated. In order to obtain a complete characterization of the samples, several different techniques such as Raman spectroscopy, AFM, SEM, EDS, TEM, SIMS and PL were used. In particular, the results obtained by SIMS suggest that the layer in which the $\beta - FeSi_2$ nanoparticles have formed is around 26.6 nm thick. The PL analysis showed that these nanoparticles emit in the near-infrared region, exhibiting a very narrow peak, with a FWHM of 1 nm, which is comparable with semiconductor laser emission. Therefore, this $\beta - FeSi_2$ nanostructured layer is potentially useful to develop near-IR lasers for fiber optics and other technological applications.

Acknowledgments

The authors are grateful to S Tehuacanero and R Hernández (IF, UNAM) for helping with the SEM and TEM operation, to M Avendaño and G Ramírez (IE-SEES, CINVESTAV-IPN) for helping with the PL and Raman measurements and to A Ángeles Pascual (LANE, CINVESTAV) for helping with the FIB sample preparation. Cecilia Salinas-Fuentes acknowledges the support of a CONACYT PhD fellowship. This work was partially supported by DGAPA-UNAM project IN100819.

ORCID iDs

Cecilia Salinas-Fuentes
https://orcid.org/0000-0002-5845-6508
Angélica Hernández-Zanabria
https://orcid.org/0000-0002-3750-5083
Yuriy Kudriavtsev
https://orcid.org/0000-0002-4122-8429
Juan-Carlos Cheang-Wong
https://orcid.org/0000-0002-1896-7864

References

[1] Antonov V N, Jepsen O, Henrion W, Rebien M, Stauss P and Lange H 1998 Electronic structure and optical properties of $\beta - FeSi_2$ *Phys. Rev.* B **57** 8934
[2] Giannini C, Lagomarsino S, Scarinci F and Castrucci P 1992 Nature of the band gap of polycrystalline $\beta - FeSi_2$ films *Phys. Rev.* B **45** 8822
[3] Lange H 1997 Electronic properties of semiconducting silicides *Phys. Status Solidi* b **201** 3–65
[4] Dimitriadis C A, Werner J H, Logothetidis S, Stutzmann M, Weber J and Nesper R 1990 Electronic properties of semiconducting $FeSi_2$ films *J. Appl. Phys.* **68** 1726–34
[5] Ishiyama T, Nakagawa S, Wakamatsu T and Fujiwara N 2018 Synthesis of $\beta - FeSi_2$ nanowires by using silicon nanowire templates *AIP Adv.* **8** 085324
[6] Terai Y, Yamaguchi H, Tsukamoto H, Murakoso N and Hoshida H 2018 Polarized Raman spectra of $\beta - FeSi_2$ epitaxial film grown by molecular beam epitaxy *AIP Adv.* **8** 105028
[7] Wang J, Leng R, Chang S, Li D and Ni H 2019 Near-infrared lateral photovoltaic effect of $\beta - FeSi_2$ films on $SrTiO_3$ substrate *Opt. Express* **27** 16521–9
[8] Rajesh P V, Das A, Ghosh B and Das D 2019 ^{57}Fe Mössbauer and XRD studies on $\beta - FeSi_2$ prepared by high energy mechanical attrition *Mater. Res. Express* **6** 085901
[9] Charoenyuenyao P, Promros N, Chaleawpong R and Yoshitake T 2018 Surface morphology and wettability for thin films of beta-iron disilicide produced through direct-current sputtering utilizing a pair of facing targets *MATEC Web of Conferences* **192** 01054
[10] Shimura K, Yamaguchi K, Yamamoto H, Sasase M, Shamoto S and Hojou K 2006 Photoluminescence of $\beta - FeSi_2$ thin film prepared by ion beam sputter deposition method *Nucl. Instrum. Methods* B **242** 673–5
[11] Shimura K, Yamaguchi K, Sasase M, Yamamoto H, Shamoto S I and Hojou K 2006 Characterization of photoluminescence of $\beta - FeSi_2$ thin film fabricated on Si and SIMOX substrate by IBSD method *Vacuum* **80** 719–22
[12] Theis J, Bywalez R, Küpper S, Lorke A and Wiggers H 2015 Charge storage in $\beta - FeSi_2$ nanoparticles *J. Appl. Phys.* **117** 054303
[13] Suemasu T, Negishi Y, Takakura K, Hasegawa F and Chikyow T 2001 Influence of Si growth temperature for embedding $\beta - FeSi_2$ and resultant strain in $\beta - FeSi_2$ on light emission from p-Si/$\beta - FeSi_2$ particles/n-Si light-emitting diodes *Appl. Phys. Lett.* **79** 1804–6
[14] Rysbaev A S, Irgashev S U, Kasimov A S, Juraeva D S, Khujaniyazov J B and Khudoyberdieva M I 2020 Optimal technological modes of ion implantation and following annealing for forming thin nanosized films of silicides *Eurasian J. Phys. Funct. Mater.* **4** 50–60
[15] Zhang F X and Saxena S 2006 Phase stability and thermal expansion property of $FeSi_2$ *Scr. Mater.* **54** 1375–7
[16] Hoshino Y, Yachida G, Yoneda T and Nakata J 2015 Silicide synthesis by Fe^+ implantation in Si substrates *Sci. J. Kanagawa University* **26** 7–12
[17] www.SRIM.org 2008
[18] Maeda Y, Umezawa K, Hayashi Y and Miyake K 2001 Raman spectroscopic study of ion-beam synthesized polycrystalline $\beta - FeSi_2$ on Si (100) *Thin Solid Films* **381** 219–24
[19] Wan Q, Wang T H and Lin C L 2003 Synthesis and optical properties of semiconducting beta-$FeSi_2$ nanocrystals *Appl. Phys. Lett.* **82** 3224–6
[20] Schuller B, Carius R and Mantl S 2003 Optical and structural properties of $\beta - FeSi_2$ precipitate layers in silicon *J. Appl. Phys.* **94** 207–11
[21] Shevlyagin A V, Goroshko D L, Chusovitin E A and Galkin N G 2016 VIS-NIR-SWIR multicolor avalanche photodetector originating from quantum-confined Stark effect in Si/$\beta - FeSi_2$/Si structure *Appl. Phys. Lett.* **109** 171101
[22] Shevlyagin A V *et al* 2017 A room-temperature-operated Si LED with $\beta - FeSi_2$ nanocrystals in the active layer: μW emission power at 1.5 μm *J. Appl. Phys.* **121** 113101
[23] He J Y, Wang X, Wu X L and Chu P K 2012 Anisotropic etching of microscale $\beta - FeSi_2$ particles: Formation, mechanism and quantum confinement of $\beta - FeSi_2$ nanowhiskers *RSC Adv.* **2** 3254–6

[24] Udono H, Kikuma I, Okuno T, Masumoto Y, Tajima H and Komuro S 2004 Optical properties of $\beta-FeSi_2$ single crystals grown from solutions *Thin Solid Films* **461** 182–7
[25] Arushanov E, Bucher E, Kloc C, Kulikova O, Kulyuk L and Siminel A 1995 Photoconductivity in n-type $\beta-FeSi_2$ single crystals *Phys. Rev.* B **52** 20
[26] Hossain M Z, Katsumata H and Uekusa S 2011 The effect of crystalline structure on photoluminescence of the $\beta-FeSi_2$ film prepared by pulsed laser deposition using two types of target *Phys. Procedia* **11** 158–62
[27] Maeda Y, Terai Y, Itakura M and Kuwano N 2004 Photoluminescence properties of ion beam synthesized $\beta-FeSi_2$ *Thin Solid Films* **461** 160–4
[28] Maeda Y 2008 Luminescence properties of $\beta-FeSi_2$ and its application to photonics *Appl. Surf. Sci.* **254** 6242–7
[29] Jiu-Yang H, Qi-Zhen Z and Xing-Long W 2013 Resonant energy transfer from nanocrystal Si to $\beta-FeSi_2$ in hybrid Si/$\beta-FeSi_2$ film *Chin. Phys.* B **22** 106804
[30] Terai Y, Nishi H and Oka N 2020 Photoluminescence properties of polycrystalline $\beta-FeSi_2$ grown by RF magnetron sputtering *Japan. J. Appl. Phys.* **59** SFFC01
[31] Arushanov E and Lisunov K G 2015 Transport properties of $\beta-FeSi_2$ *Japan. J. Appl. Phys.* **54** 07JA02
[32] Okajima K, Yamatsugu H, Wen C, Sudoh M and Yamada K 2001 Spectral sensitivity enhancement by thin film of $\beta-FeSi_2$–Si composite prepared by RF-sputtering deposition *Thin Solid Films* **381** 267–75
[33] Maeda Y, Tatsumi T, Kawakubo Y, Noguchi Y, Kobayashi H, Narumi K and Sakai S 2014 Enhancement of IR photoluminescence of $\beta-FeSi_2$ nanocrystals by Cu-doping and study of its mechanism *Phys. Status Solidi* C **11** 1626–9